CANCER

Oncogenic role of a developmentally regulated *NTRK2* splice variant

Siobhan S. Pattwell[1,2,3]*, Sonali Arora[1], Nicholas Nuechterlein[4], Michael Zager[5,6], Keith R. Loeb[7,8], Patrick J. Cimino[1,8], Nikolas C. Holland[9,10], Noemi Reche-Ley[11]‡, Hamid Bolouri[1,12], Damian A. Almiron Bonnin[1], Frank Szulzewsky[1], Vaishnavi V. Phadnis[13]†, Tatsuya Ozawa[14], Michael J. Wagner[7,15], Michael C. Haffner[1,7,8], Junyue Cao[16], Jay Shendure[5,17,18,19], Eric C. Holland[1,20]§

Temporally regulated alternative splicing choices are vital for proper development, yet the wrong splice choice may be detrimental. Here, we highlight a previously unidentified role for the neurotrophin receptor splice variant TrkB.T1 in neurodevelopment, embryogenesis, transformation, and oncogenesis across multiple tumor types in humans and mice. TrkB.T1 is the predominant *NTRK2* isoform across embryonic organogenesis, and forced overexpression of this embryonic pattern causes multiple solid and nonsolid tumors in mice in the context of tumor suppressor loss. TrkB.T1 also emerges as the predominant *NTRK* isoform expressed in a wide range of adult and pediatric tumors, including those harboring tropomyosin receptor kinase fusions. Affinity purification–mass spectrometry proteomic analysis reveals distinct interactors with known developmental and oncogenic signaling pathways such as Wnt, transforming growth factor–β, Sonic Hedgehog, and Ras. From alterations in splicing factors to changes in gene expression, the discovery of isoform specific oncogenes with embryonic ancestry has the potential to shape the way we think about developmental systems and oncology.

INTRODUCTION

Embryogenesis and neurodevelopment, in particular, comprise an elegant and well-orchestrated series of tightly regulated events, culminating in an organized and highly functioning organism. Cancer, on the other hand, can often be viewed as an uncontrolled, unrestrained, genetically chaotic disease, lacking the precise spatial and temporal rigidity associated with normal development. While appearing to be on opposite sides of the organizational spectrum, the similarities between early development and oncogenesis are numerous. This has been observed frequently as key developmental signaling pathways, such as Wnt, Hedgehog, or Notch, have been shown to be dysregulated in cancer across all stages from tumor initiation and maintenance to metastasis (*1*).

Encoded by the *NTRK2* gene, the tropomyosin receptor kinase TrkB, which has many alternatively spliced isoforms, has well-established roles across neurodevelopment and astrocyte biology and has also been implicated in a wide range of cancer types (*2*–*23*). *NTRK2* gene fusions have recently been the focus of many clinical and pharmacological studies (*24*–*27*), while inhibition of the TrkB kinase has been shown to inhibit cell proliferation and contribute to apoptosis (*7*). In addition to well-known roles in neurobiology, recent studies suggest that *NTRK2* may render cells resistant to anoikis and prone to metastasis, while others suggest its involvement in the epithelial-to-mesenchymal transition associated with increased migration and invasiveness of many cancer cell lines (*6*, *8*, *9*, *28*–*32*), yet the precise mechanisms of how TrkB exerts its oncogenic role are not fully known. While prior studies have been fundamental in uncovering *NTRK2* involvement in cancer, the complex posttranslational modifications intricate splicing patterns, and prior roles in embryogenesis are often ignored.

Recent findings have shown that a kinase-deficient *NTRK2* splice variant, TrkB.T1, is the predominant neurotrophin receptor in human gliomas, enhances glioma aggressiveness in mice, and increases the perdurance of platelet-derived growth factor (PDGF)–induced Akt and signal transducers and activators of transcription 3 (STAT3) signaling (*33*). This splice variant contains a unique terminal exon encoding a 11–amino acid tail that is 100% conserved across species including chicks, mice, rats, felines, and humans (*34*–*39*), suggesting a potential evolutionarily important biological role. In light of recent findings implicating this kinase-deficient splice variant in glioma biology (*33*), we explore the role of TrkB.T1 in neural development and early embryonic central nervous system (CNS) and mesenchymal development in particular.

[1]Human Biology Division, Fred Hutchinson Cancer Research Center, 1100 Fairview Avenue North, Mailstop C3-168, Seattle, WA 98109, USA. [2]Ben Towne Center for Childhood Cancer Research, Seattle Children's Research Institute, Seattle, WA 98101, USA. [3]Division of Pediatrics, Department Hematology/Oncology, University of Washington School of Medicine, Seattle, WA 98105, USA. [4]Paul G. Allen School of Computer Science & Engineering, University of Washington, Seattle, WA 98195, USA. [5]Brotman Baty Institute for Precision Medicine, Seattle, WA 98195, USA. [6]Center for Data Visualization, Fred Hutchinson Cancer Research Center, Seattle, WA 98109, USA. [7]Clinical Research Division, Fred Hutchinson Cancer Research Center, 1100 Fairview Avenue North, Seattle, WA 98109, USA. [8]Department of Laboratory Medicine and Pathology, University of Washington School of Medicine, 325 9th Avenue, Box 359791, Seattle, WA 98104, USA. [9]Center for Neural Science, New York University, 4 Washington Place, #809, New York, NY 10003, USA. [10]Department of Psychiatry, Weill Cornell Medical College, 1300 York Ave, New York, NY 10065, USA. [11]The Bush School, 3400 E Harrison St, Seattle, WA 98112, USA. [12]Benaroya Research Institute, 1201 Ninth Avenue, Seattle, WA 98101, USA. [13]Whitehead Institute for Biomedical Research, Cambridge, MA 02142, USA. [14]Division of Brain Tumor Translational Research, National Cancer Center Research Institute, 5-1-1 Tsukiji, Chuo-ku, Tokyo 104-0045, Japan. [15]Division of Medical Oncology, University of Washington, 825 Eastlake Ave E., Seattle, WA 98109, USA. [16]Rockefeller University, 1230 York Ave, New York, NY 10065, USA. [17]Department of Genome Sciences, University of Washington, Seattle, WA 98195, USA. [18]Allen Discovery Center for Cell Lineage Tracing, Seattle, WA 98195, USA. [19]Howard Hughes Medical Institute, Seattle, WA 98195, USA. [20]Seattle Tumor Translational Research Center, Fred Hutchinson Cancer Research Center, 1100 Fairview Avenue North, Seattle, WA 98109, USA.
*Corresponding author. Email: eholland@fredhutch.org (E.C.H.); spattwel@fredhutch.org, siobhan.pattwell@seattlechildrens.org, pattwell@uw.edu (S.S.P.)
†Present address: Harvard Medical School, 25 Shattuck St, Boston, MA 02115, USA.
‡Present address: Stanford University, 450 Serra Mall, Stanford, CA 94305, USA.
§Present address: 1 Bungtown Rd, Cold Spring Harbor, NY 11724, USA.

In this study, we characterize the role of the *NTRK2* splice variant, TrkB.T1, in embryonic neurodevelopment and early organogenesis via transcript analysis of an enhanced single-cell combinatorial indexing RNA sequencing analysis method (sci-RNA-seq3) data of embryonic day 9.5 (E9.5) to E13.5 mouse embryos (*40*) and transcript-specific immunohistochemistry. We demonstrate a developmental role for TrkB.T1 beyond that of the CNS, highlight TrkB.T1's transformation potential in vitro, and uncover its role as an oncogenic driver in vivo using a RCAS-TVA mouse model (*41*, *42*). We further reveal TrkB.T1 to be the predominant TRK isoform expressed across the majority of adult and pediatric tumors using clinical data from The Cancer Genome Atlas (TCGA) (*43*) and the Therapeutically Applicable Research to Generate Effective Treatments (TARGET) initiative, respectively, and uncover a several potential interactors via proteomic analysis. Using TrkB.T1, we explore the role of developmentally regulated splicing choices and subsequently show that forced expression of a specific isoform can be neoplastic in the same postnatal organs that once expressed it during embryogenesis. This kinase-deficient splice variant of *NTRK2* is found across normal embryonic development and is a driver of cancer in vivo when overexpressed postnatally in many of the cell types that expressed it during embryonic development.

RESULTS

TrkB.T1 in embryonic development and organogenesis

It is widely known that the majority of organ development in rodents occurs before E18 (*40*) and recent advances in next-generation sequencing have allowed for the characterization of transcriptional dynamics across development at a single-cell resolution resulting in the Mouse Organogenesis Cell Atlas (MOCA) (*40*). To explore the expression of TrkB.T1 in CNS development, we used the fact that the TrkB.T1 and full-length TrkB.FL *NTRK2* transcripts differ in their 3′ ends (*38*), which allows for transcript quantification in single-cell RNA sequencing data and mapped expression of individual transcripts in mouse embryos over developmental time. Specifically, TrkB.T1 is not the result a pure truncation and contains a uniquely spliced in exon that is not present in the full-length, kinase-containing variant (Fig. 1A). TrkB.FL contains several exons downstream of this exon that are not present in TrkB.T1 (Fig. 1A), allowing for quantification of these two alternative spliced variants in our dataset (*38*). Using sci-RNA-seq3 data, the MOCA (*40*) provides gene expression data and cell trajectory annotation for 2,026,641 cells from 61 mouse embryos across five development stages (E9.5 to E13.5), resulting in 38 main cell clusters and 10 main trajectories. The expression of transcripts for all protein coding genes, including TrkB.T1 and TrkB.FL, was normalized and visualized over the existing landscape provided by Cao *et al.* (*40*). First, we examined TrkB.FL expression patterns in the *t*-distributed stochastic neighbor embedding (*t*-SNE) plot of all 38 cell types within the MOCA and found that TrkB.FL expression is appreciably restricted to a subset of cell types, all of which were neuronal in nature (Fig. 1, B and C, and fig. S1, A to E). TrkB.T1, however, was expressed broadly across many different cell types within the embryo during this period (Fig. 1, D and E, and fig. S1, F to J). We next sought to explore the *NTRK2* transcript expression patters within the CNS developmental trajectory and found that TrkB.T1 cellular expression is observed across multiple neurodevelopmentally driven cell clusters, including radial glia, immature oligodendrocytes, and isthmic organizer cells (Fig. 1F). The second largest population of cells with high variable levels of TrkB.T1 expression during this developmental period is found in the mesenchymal trajectory, and mapping expression of both transcripts showed a vast predominance of TrkB.T1 over TrkB.FL similar to the nonneuronal cell types of the developing CNS (Fig. 1, F to I). Visualization of *NTRK2* expression reveals intense, diffuse patterns of TrkB.T1 across multiple days in multiple cell types, with expression levels rivaling those of actin in particular clusters (figs. S1, F to J, and S2), whereas TrkB.FL expression remains predominantly restricted to mature neurons (fig. S1, A to E). An interactive site allowing three-dimensional visualization and further exploration of *NTRK2* transcripts among cell types and within the CNS and mesenchymal trajectories over developmental time can be found at https://atlas.fredhutch.org/fredhutch/ntrk2/.

As the sci-RNA-seq3 data show widespread TrkB.T1 expression across multiple clusters within and outside the CNS, we wanted to visualize TrkB.T1 and TrkB.FL expression across embryonic development beyond E13.5. To this end, we stained histological sections of embryos from E10 to E17 with antibodies specific to the TrkB.FL kinase domain and an antibody specific to the intracellular 11–amino acid tail of TrkB.T1 (*44*). Similar to the sci-RNA-seq3 data, examination at early embryonic time points, when the most rapid cellular growth and organogenesis are underway, the protein ratio between these two receptors is different, with TrkB.T1 present at exceedingly high levels in multiple organ sites (Fig. 2, A to I) compared to TrkB.FL (Fig. 2, J to R), which is predominantly expressed and maintained in CNS only, consistent with the transcript levels for the two TrkB gene products shown in Fig. 1. By the end of embryonic development circa E17, immunohistochemistry of both splice variants reveals that TrkB.T1 levels have decreased but are still present throughout various non-CNS organs, while the majority of TrkB.FL remains restricted within the CNS (Fig. 2). These data suggest that in addition to known roles in CNS development and gliomagenesis, TrkB.T1 may have a more widespread role in early organogenesis throughout the developing organism. Since TrkB.T1 has been shown to play a role brain tumors (*33*), this widespread embryonic expression pattern suggests that TrkB.T1's roles, in both development and cancer, may not be restricted to the CNS, highlighting the possibility that it may also influence additional tumor types beyond what has been shown for gliomas.

TrkB.T1 exerts significantly more transformation capacity compared to TrkB.FL in colony formation assay and is required for neurosphere formation

Given the widespread distribution of TrkB.T1 in multiple organ sites and cell types across embryonic development and our recent findings that the TrkB.T1 splice variant predominates over the full-length kinase-containing TrkB variant in gliomas and that this TrkB.T1 gene product enhances PDGF-driven glioma aggressiveness in vivo and amplifies PDGF-driven AKT and Stat signaling in vitro (*44*), we wanted to compare the relative transformation potential of the kinase-containing TrkB.FL and kinase-deficient TrkB.T1 isoforms in a gain-of-function experiment using a soft agar colony formation assay. Forced expression of the TrkB.T1 splice variant containing its unique 11–amino acid intracellular tail in 3T3 cells led to significantly enhanced colony formation (average colonies = 209) compared to overexpression of the kinase-containing variant, TrkB.FL (average colonies = 48), or control vector (average colonies = 19.33) [$F(2,6) = 401.5$, $P < 0.0001$) (Fig. 3A). Using a short hairpin designed against

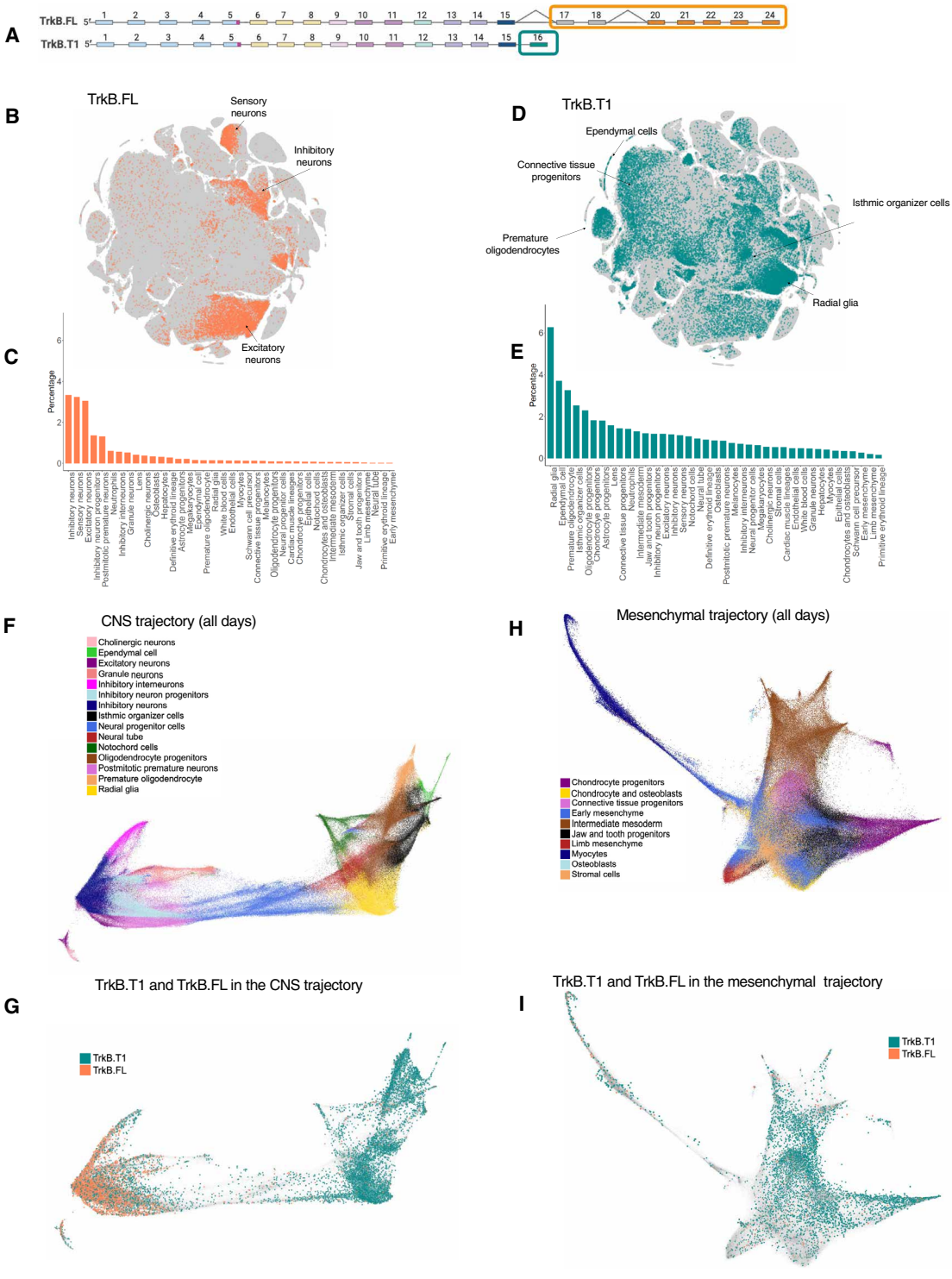

Fig. 1. sci-RNA-seq3 transcript analysis across E9.5 to E13.5 mouse embryonic development shows TrkB.FL expression in neuronal clusters with widespread TrkB.T1 expression in CNS and mesenchymal trajectories. (**A**) Schematic depicting two alternatively spliced *NTRK2* transcripts (TrkB.T1 and TrkB.FL) shows unique exons present in each variant. *t*-SNE visualization of TrkB.FL expression (**B** and **C**) and TrkB.T1 (**D** and **E**) of 2,026,641 mouse embryo cells from E9.5 to E13.5 (*40*) shows high TrkB.FL expression in neuronal clusters and CNS clusters with strong, diffuse TrkB.T1 expression across the majority of cell clusters. Visualization of CNS (**F**) and mesenchymal (**G**) cell type trajectories across all days shows strong expression of TrkB.FL in mature neuronal cells (**H**) with diffuse expression of TrkB.T1 in large subsets of immature stem-like cells across developmental trajectories (**I**).

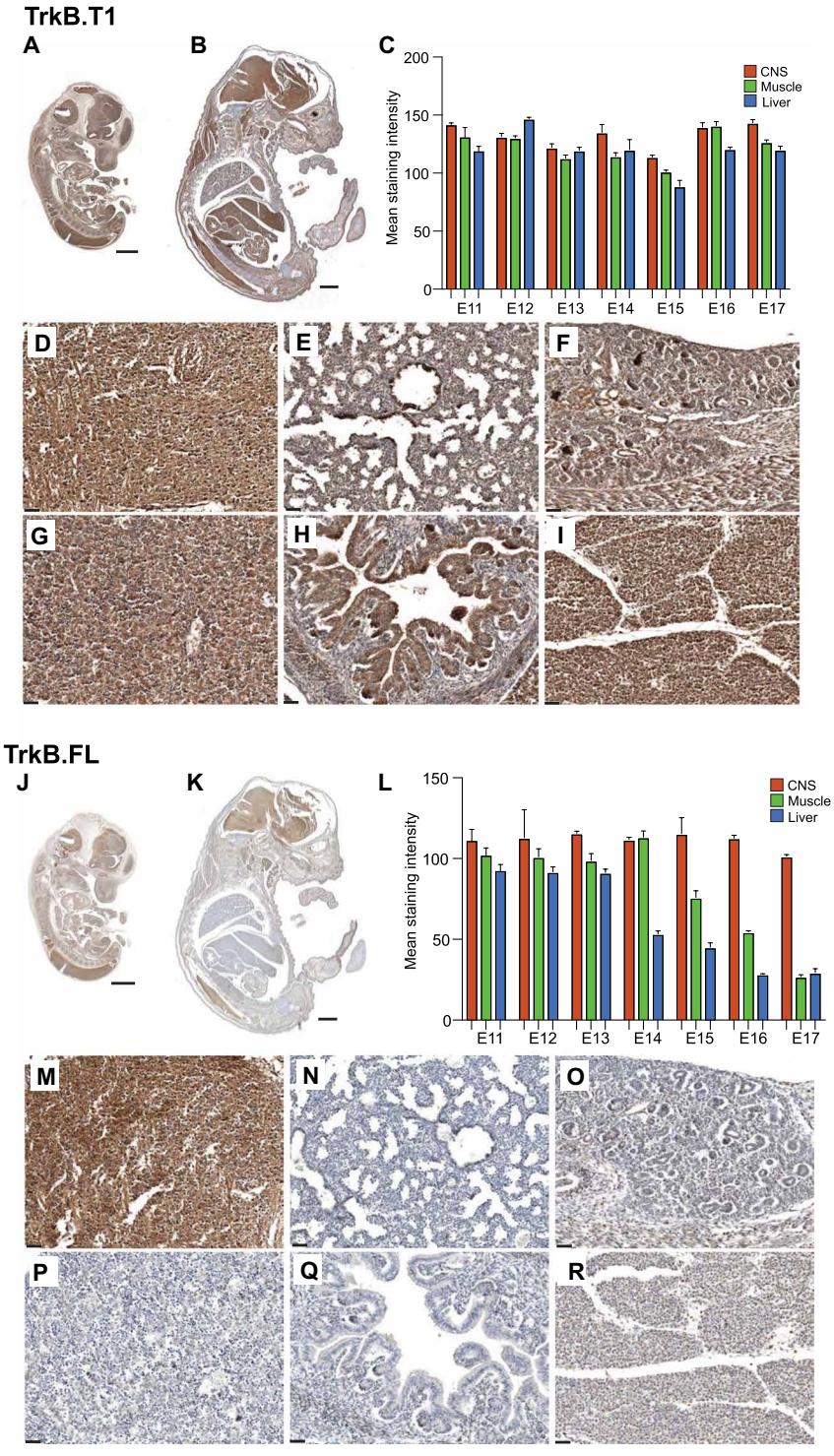

Fig. 2. TrkB transcript expression across E10 to E17 embryonic development. Representative micrographs of immunohistochemical staining of TrkB.T1 in the whole-mount murine embryo section at E11 (**A**) and E16 (**B**). Quantitative assessment of staining intensities in CNS (red), muscle (green), and liver (blue) at different developmental stages (**C**). Representative micrographs for TrkB.T1 staining of the (**D**) brain, (**E**) lung, (**F**) kidney, (**G**) liver, (**H**) small intestine, (**I**) skeletal muscle at E16. Immunohistochemical staining of TrkB.FL in the whole-mount embryo section at E11 (**J**) and E16 (**K**) with (**L**) quantitative assessment of staining intensities in the CNS (red), muscle (green), and liver (blue) at different developmental stages. Representative micrographs for TrkB.FL staining in the (**M**) brain, (**N**) lung, (**O**) kidney, (**P**) liver, (**Q**) small intestine, (**R**) skeletal muscle at E16. Scale bars, 1 mm (A, B, J, and K) and 100 μm (D to I and M to R).

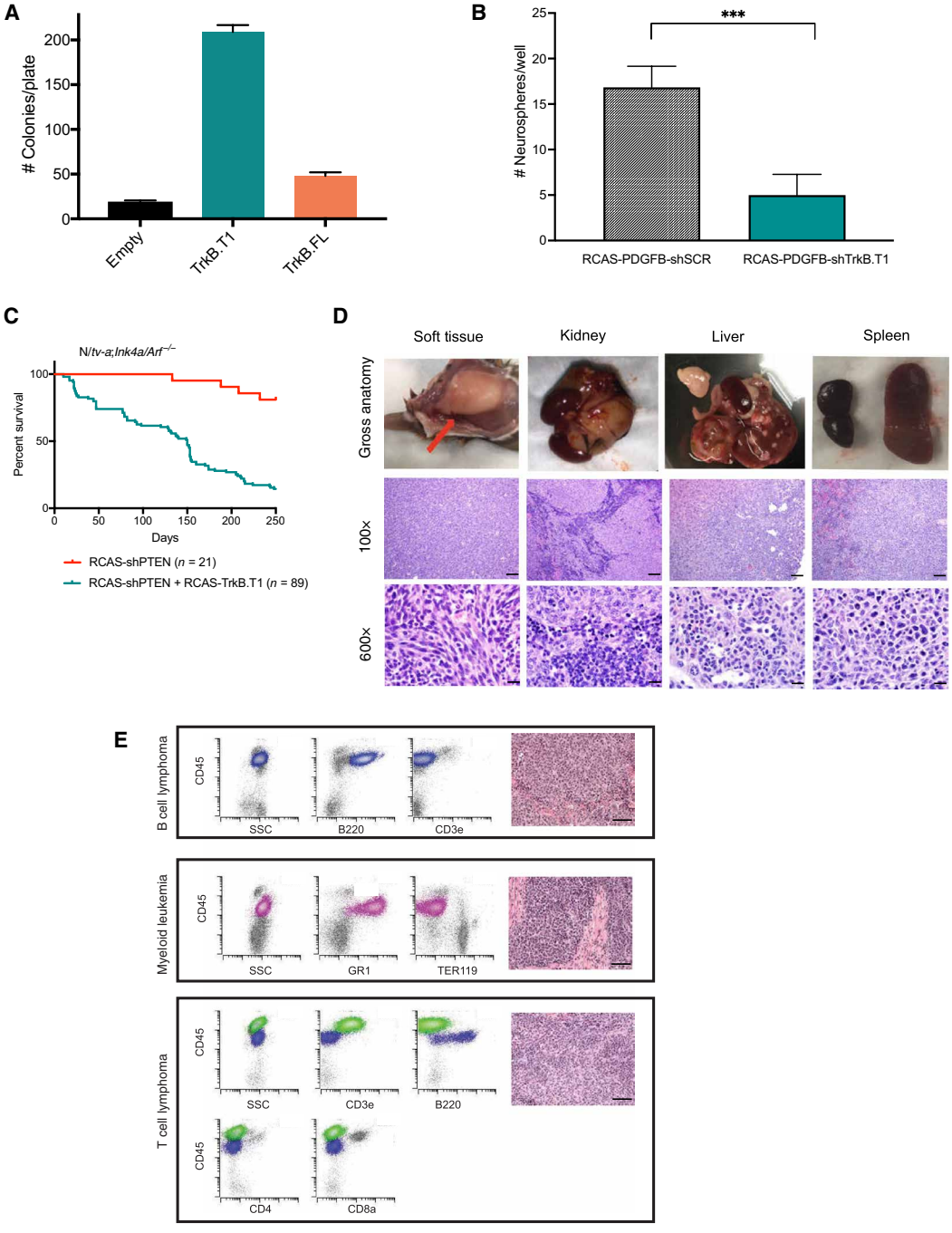

Fig. 3. Gain- and loss-of-function experiments show that TrkB.T1 transforms 3T3 cells, is required for neurosphere formation, and causes solid and nonsolid tumors throughout the body in mice when overexpressed in the context of tumor suppressor loss. (**A**) Soft agar colony formation assay in 3T3 cells shows significantly increased colonies with TrkB.T1 compared to control and TrkB.FL ($P < 0.0001$; graph represents means + SEM). (**B**) TrkB.T1 knockdown with RCAS-PDGFB-shTrkB.T1 significantly decreases neurosphere formation in primary Nestin/*tv-a*;*Ink4a/Arf*$^{-/-}$ NSCs (RCAS-PDGFB-shTrkB.T1: $M = 16.833 + SD\ 2.317$ versus RCAS-PDGFB-shSCR: $M = 5.000 + SD\ 2.280$; $t(5) = 11.31$, $P < 0.0001$). Survival curves for Nestin/*tv-a*;*Ink4a/Arf*$^{-/-}$ mice injected with RCAS-shPTEN alone or RCAS-shPTEN + RCAS-TrkB.T1 (**C**) demonstrate decreases in survival due to tumor burden outside the CNS for mice injected with RCAS-TrkB.T1 + RCAS-shPTEN versus RCAS-shPTEN alone (median survival, 131 versus 250 days; log-rank hazard ratio, 0.07243; 95% confidence interval, 0.0.04768 to 0.11; $P < 0.0001$) including the soft tissue, kidney, liver, and spleen as shown in (**D**) and (**E**). Scale bars, 100 μm (100×) and 20 μm (600×). Flow cytometry analysis of splenic tumor demonstrates a large B cell lymphoma [(CD45 bright/B220$^+$; blue population) with diffuse collection of large atypical cells with vesicular chromatin and high mitotic rate with a vague nodular pattern], myeloid leukemia [(CD45$^+$/GR1$^+$; pink population) with extramedullary erythropoiesis (Ter119$^+$/dim CD45; gray population), showing focal collections of intermediate size cells with open chromatin and frequent mitosis, admixed with maturing erythroid cells], and an abnormal T cell population [(CD45 bright/CD3e$^+$/CD4$^-$/CD8a$^-$; green population) consistent with a T cell lymphoma admixed with reactive B cells (CD45 bright/B220 variable; blue population), showing large atypical cells with a high mitotic rate admixed with scattered small reactive lymphocytes and eosinophils] (20×). Scale bars, 50 μm. ***$P < 0.0001$.

TrkB.T1 to explore loss of function, we show that TrkB.T1 is necessary for neurosphere formation of primary *N/tv-a*;*Ink4a/Arf*$^{-/-}$ neural stem cells (NSCs) and that knocking down TrkB.T1 with RCAS-PDGFB-shTrkB.T1 in primary NSCs leads to significantly less neurosphere formation compared to RCAS–PDGFB–shScrambled (SCR) control (Fig. 3B and fig. S3).

Forced postnatal expression of TrkB.T1 causes multiple cancer types in mice

Prior investigation into TrkB.T1's role in gliomas revealed that a multitude of genes in phosphatidylinositol 3-kinase (PI3K)/Akt/phosphatidylinositol phosphate/inositol phosphate pathways were significantly positively correlated with *NTRK2* expression in low grade glioma (LGG) and glioblastoma multiforme (GBM) compared to normal brain (*44*) via differential gene correlation analysis (DGCA), suggesting a role for TrkB.T1 in the PI3K signaling pathway. On the basis of these results, we wanted to explore whether TrkB.T1 is capable of inducing tumors within and outside the CNS in the context of *PTEN* loss, because Pten (phosphatase and tensin homolog) is a negative regulator of Akt. We chose mice with a sensitized background [*CDKN2A* (Ink4a/Arf) loss, as this is a frequent event in multiple cancers] because TrkB.T1 overexpression does not cause tumors on its own in wild-type mice (*33*). To answer this question of whether TrkB.T1 causes tumors outside the CNS, we used the RCAS/TVA system, which allows for somatic expression of a gene of interest in particular cell types, to force overexpression TrkB.T1 and knockdown *PTEN* expression in nestin-positive progenitor cells of Ink4a/Arf$^{-/-}$ mice (*41*).

Misexpression of factors or proteins that are benign or necessary in one cell type may lead to aberrant and noncanonical signaling in another cell type, as has been shown for Wnt signaling (*45*). Because nestin is expressed in a wide range of stem and progenitor cells during the development of various organ sites (not just neural and glial progenitors), this promoter was chosen to target RCAS delivery specifically to nestin-positive cells. *N/tv-a*;*Ink4a/Arf*$^{-/-}$ mice were injected intraperitoneally or intramuscularly with RCAS-TrkB.T1 and RCAS-shPTEN. While neither RCAS-shPTEN nor RCAS-TrkB.T1 alone caused cancer in this genetic background during the time course of this experiment, the combination of RCAS-shPTEN and RCAS-TrkB.T1 injections caused a range of solid and nonsolid tumors originating from nestin-positive cells outside of CNS (Fig. 3C). These included soft tissue sarcomas, carcinomas arising in the kidney, and lymphoid leukemias and lymphomas (Fig. 3, D and E). Because our RCAS-TrkB.T1 + RCAS-shPTEN–injected mice exhibited a wide range of tumor types (sarcomas, kidney, liver, nonsolid tumors, etc.), we injected many more mice in this cohort than was needed for statistically significant survival differences so that we could ultimately have a wide range of tumor types for subsequent histological analyses. Immunohistochemistry on these solid tumors confirmed that these tumors throughout the body had both high levels of TrkB.T1 and loss of PTEN expression (fig. S4, A to D), demonstrating that forced expression of TrkB.T1 in combination with PTEN loss has the potential to form tumors in the same organ sites that once expressed TrkB.T1 embryonically.

Proteomic analysis reveals TrkB.T1-specific interactors with known developmental, oncogenic, and cell cycle signaling pathways

We explored potential interactors and up-regulated pathways in an isoform-specific *NTRK2* manner in 3T3 cells separately transduced with pLJM1-lentiviral vectors containing either TrkB.T1–hemagglutinin (HA) or TrkB.FL-HA (*46*, *47*) in the presence or absence of serum. Lysates were collected and subjected to HA-tag pull-down and subsequent affinity purification–mass spectrometry (AP-MS) proteomic analysis (*48*) to reveal potentially directly or indirectly interacting proteins (*48*).

Using HA-tagged *NTRK2* splice variants as bait, all immunoprecipitated proteins were identified, quantified, characterized, and subjected to Gene Ontology (GO) and Reactome pathway enrichment analysis to understand and explore potential protein-protein interactions (Fig. 4). In the absence of serum, TrkB.FL-expressing 3T3 cells began to die off, while TrkB.T1 cells continued to thrive, similar to the enhanced growth observed in the colony formation assay (Fig. 3A). For these serum-starved conditions, 163 shared proteins were pulled down in complexes with both TrkB.T1 and TrkB.FL, 110 were pulled down specifically with TrkB.FL, and 720 proteins were pulled down specifically in complexes with TrkB.T1. Under normal culture conditions, in the presence of serum, 749 proteins were pulled down in complexes with both TrkB.T1 and TrkB.FL, 399 were pulled down specifically with TrkB.FL, and 565 proteins were pulled down specifically in complexes with TrkB.T1 (dataset S1). GO and Reactome pathway enrichment analyses on these clusters of affinity-purified proteins revealed differential expression of a host of developmental, oncogenic, and mitotic pathway terms associated specifically with TrkB.T1 in the presence or absence of serum compared to the terms associated with TrkB.FL (fig. S5 and dataset S1). Shared developmental and oncogenic terms between TrkB.T1 and TrkB.FL in the presence of serum implicated proteins or classes of proteins involved in fibroblast growth factor receptor 2 (FGFR2), insulin-like growth factor receptor (IGFR), SLITs, Roundabout (ROBO), Sonic Hedgehog (SHH), tumor protein 53 (TP53), and runt-related transcription factor (RUNX) signaling, long known to be associated with neurotrophin signaling. Additional classes of proteins were found to be TrkB.T1 specific under normal culture conditions and maintained in the absence of serum. Among these TrkB.T1-specific interactors ($n = 565$) are proteins with known developmental and oncogenic roles, including Gli, Hedgehog, Wnt, transforming growth factor–β (TGF-β), Ras, mitogen-activated protein kinase (MAPK), MET, calmodulin (CaM), and other signaling pathways (Fig. 4, fig. S5, and dataset S1). The distinct protein sets were pulled down with TrkB.T1 highlight a host of developmental, oncogenic, and cell cycle/cell division pathway binding partners that were not previously known to interact with TrkB.T1 along with several known interactors such as those associated with RhoA (*49*, *50*) and Ca^{2+} signaling (*51*).

TrkB.T1 is the predominantly expressed form of TrkB RNA and protein in adult and pediatric tumors

The large number and breadth of murine tumor types induced by TrkB.T1 expression, combined with the knowledge that, in gliomas, the predominant form of TrkB is the TrkB.T1 splice variant, prompted an in-depth pan-cancer analysis of *NTRK2* transcript expression across all organ sites within TCGA. Similar to what has been reported for gliomas (*44*), expression of the full-length, kinase-containing TrkB.FL is minimal to absent across the majority of tumor types within TCGA, while TrkB.T1 expression is consistently high (Fig. 5 and dataset S2). In-depth transcript characterization of all TCGA tumors harboring known NTRK fusions recapitulates this pattern and shows that, regardless of TRK fusion (NTRK1, NTRK2, and NTRK3), expression of the TrkB.T1-specifiic exon (encoding for

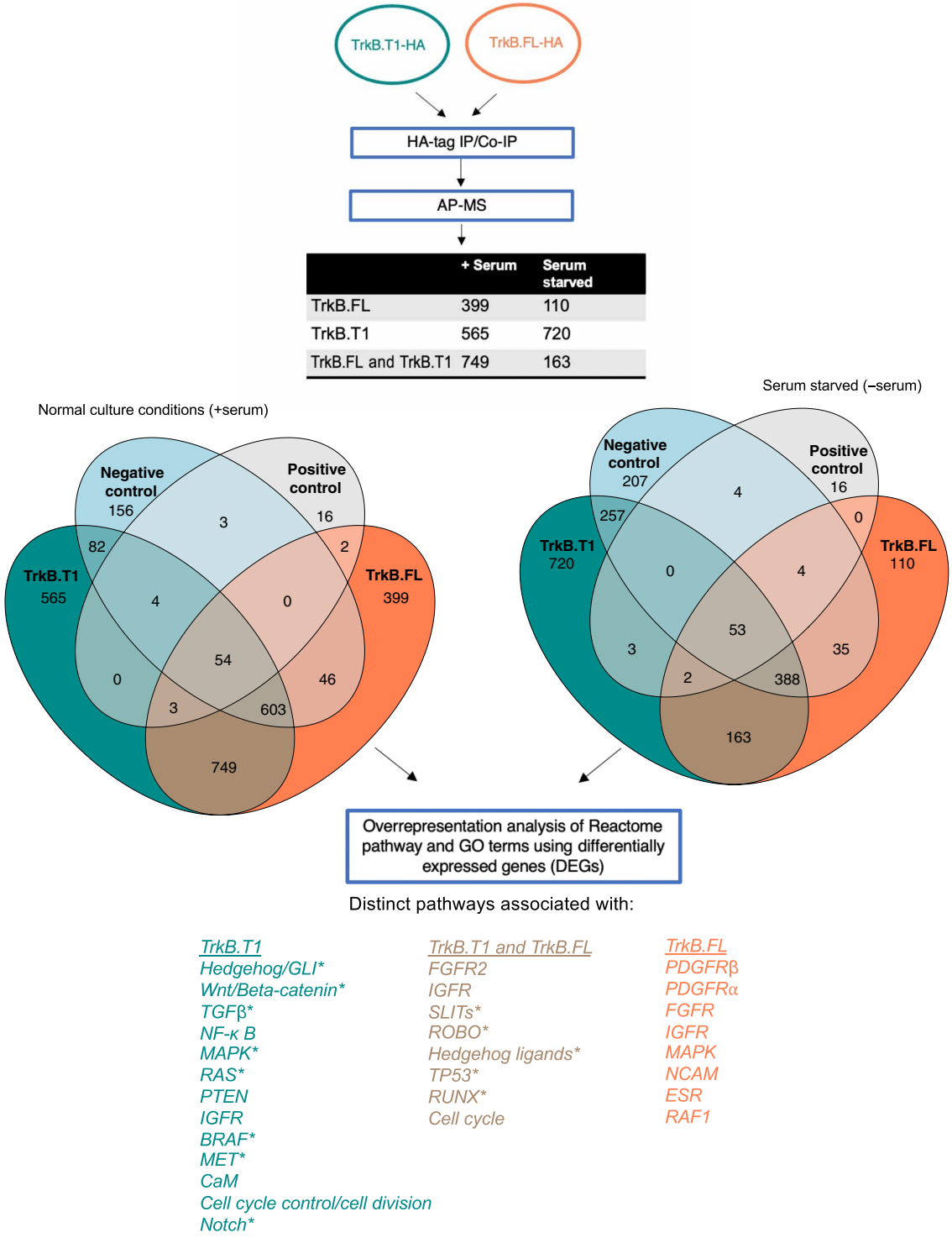

Fig. 4. AP-MS spectrometry reveals *NTRK2* splice variant interactors associated with developmental and oncogenic pathways. 3T3 cells were transduced with TrkB.T1-HA or TrkB.FL-HA, each in triplicate, and subjected to HA pull-down to identify direct and indirect interactors via AP-MS as shown in fig. S3 and dataset S1. Proteins specific to each isoform and shared between both isoforms (with serum: $n = 599$ for TrkB.T1, $n = 399$ for TrkB.FL, and $n = 749$ shared; without serum: $n = 720$ for TrkB.T1, $n = 110$ for TrkB.FL, and $n = 163$ shared) were subjected to GO and Reactome pathway enrichment analysis to find proteins associated with developmental, oncogenic, and cell cycle/cell division pathways. *Developmental, oncogenic, and cell cycle/cell division–associated signaling pathways listed are associated under normal culture conditions (with serum) unless shown with asterisk, which denotes that proteins associated with these pathways were found both under normal culture conditions and serum-starved conditions.

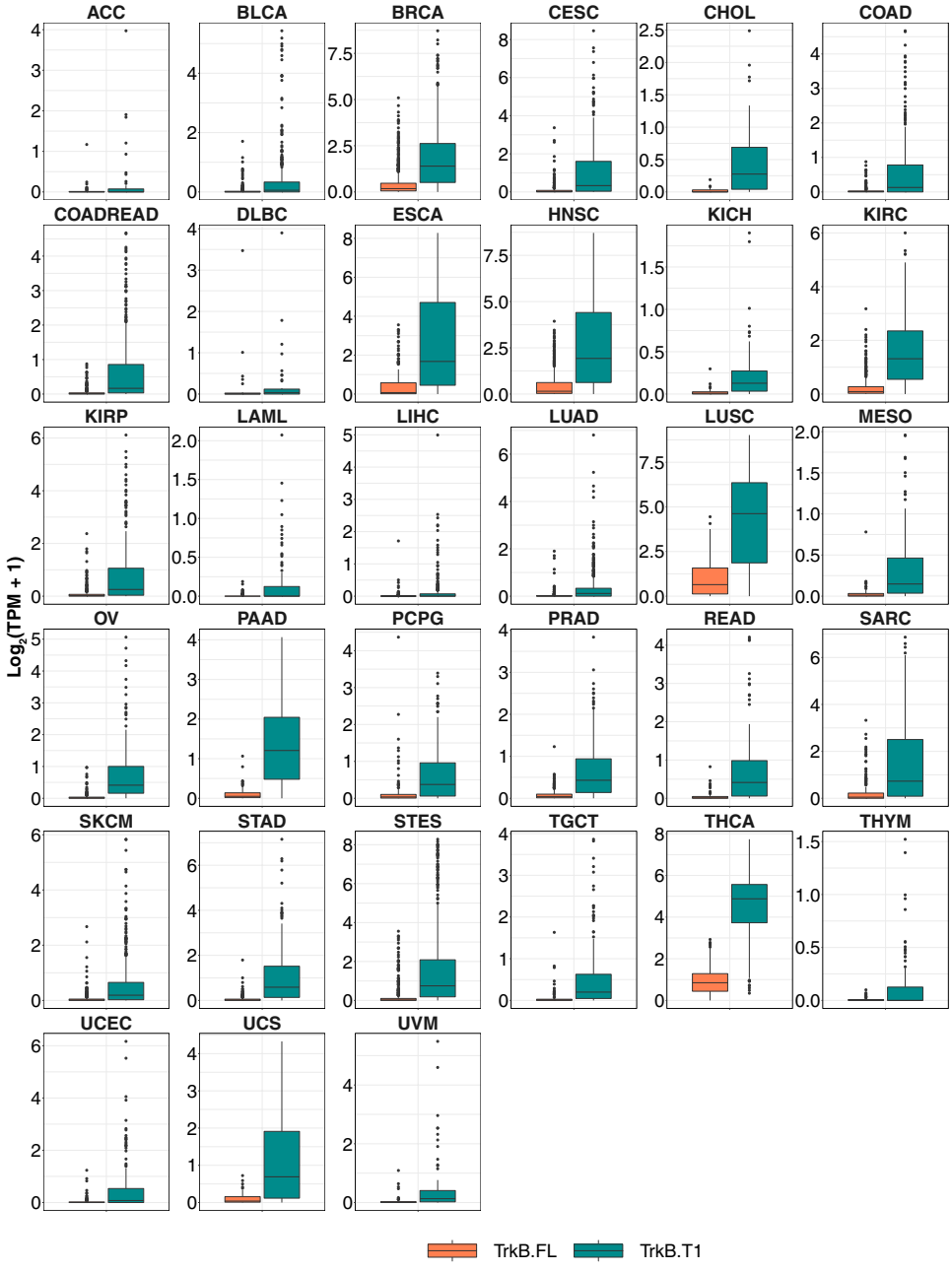

Fig. 5. Pan-cancer *NTRK2* transcript analyses. *NTRK2* transcript analysis shows minimal to zero expression of TrkB.FL transcript and increased expression for TrkB.T1 transcript across all TCGA organ sites: adrenocortical carcinoma (ACC), bladder urothelial cancer (BLCA), breast invasive carcinoma (BRCA), cervical squamous cell carcinoma and endocervical adenocarcinoma (CESC), cholangiocarcinoma (CHOL), colon adenocarcinoma (COAD), colorectal adenocarcinoma (COAD/READ), lymphoid neoplasm diffuse B cell lymphoma (DLBC), esophageal carcinoma (ESCA), head and neck squamous carcinoma (HNSC), kidney chromophobe (KICH), kidney renal clear cell carcinoma (KIRC), kidney renal papillary cell carcinoma (KIRP), acute myeloid leukemia (LAML), liver hepatocellular carcinoma (LIHC), lung adenocarcinoma (LUAD), lung squamous cell carcinoma (LUSC), mesothelioma (MES), ovarian serous cystadenocarcinoma (OV), pancreatic adenocarcinoma (PAAD), pheochromocytoma and paraganglioma (PCPG), prostate adenocarcinoma (PRAD), rectum adenocarcinoma (READ), sarcoma (SARC), skin cutaneous melanoma (SKCM), stomach adenocarcinoma (STAD), stomach and esophageal (STES), testicular germ cell tumor (TGCT), thyroid carcinoma (THCA), thymoma (THYM), uterine corpus endometrial carcinoma (UCEC), uterine carcinoma (UCS), and uveal melanoma (UVM). Data are represented as boxplots where the middle line is the median, the lower and upper hinges correspond to the first and third quartiles (the 25th and 75th percentiles), the upper whisker extends from the hinge to the largest value no further than 1.5× IQR from the hinge (where IQR is the interquartile range or distance between the first and third quartiles), and the lower whisker extends from the hinge to the smallest value at most 1.5× IQR of the hinge, while data beyond the end of the whiskers are outlying points that are plotted individually.

the unique 11–amino acid intracellular region) remains consistently higher than all kinase-containing TRK exons, regardless of the particular TRK fusion or tumor type (fig. S6 and dataset S3).

To extend upon these transcript results demonstrating predominant TrkB.T1 expression across a wide range of human tumors, we next determined how well RNA transcripts correlate with TrkB.T1 protein distribution. Immunohistochemistry on a tissue microarray of various adult tumors (Fig. 6) reveals variable, increased TrkB.T1 expression and distribution, with high TrkB.T1 *H* score values (dataset S4) for nearly all tumor types. These results show that both RNA transcript expression and protein levels for TrkB.T1 are high across all tumor types in available datasets, suggesting that this is the *NTRK2* splicing choice made across cancers and predominates in nonneuronal cells of the embryo as well.

In addition to immunohistochemistry (Fig. 6) and the data from TCGA, which is composed of mostly adult tumors, previous studies have also shown a potential role for TrkB in pediatric tumors, and its gene products have been shown to be expressed at high levels in high-risk neuroblastoma (NBL) and correlated with poor prognosis (*29*, *52*), while levels of TrkB gene products have been shown to be correlated with unfavorable outcome in patients with Wilms tumor (WT) (*15*). Transcript-specific analysis of pediatric data from the TARGET program confirms that, similar to adult tumors in TCGA, TrkB.T1 expression is the predominant isoform compared to TrkB.FL in several cancer types, including WT, rhabdoid tumor, NBL, and clear-cell sarcoma of the kidney (fig. S7 and dataset S2).

Together, these data show that TrkB.T1 is the *NTRK2* isoform expressed in multiple cell types across embryonic development, is expressed at unexpectedly high rates across adult and pediatric cancers from multiple sites within TCGA and TARGET (Fig. 5, fig. S7, and datasets S2 to S4), and is capable of transforming cells in vitro and causing tumors across various organ sites in the context of loss of the common tumor suppressors Ink4a/Arf and PTEN in mice (Fig. 3 and fig. S4), potentially through its interactions with known oncogenic and developmental signaling pathways (fig. S5 and dataset S1). These data highlight the TrkB.T1 splice variant as one candidate whose aberrant expression with concurrent tumor suppressor loss causes cancer in the same developed organs where it played a role in early embryonic development.

DISCUSSION

While many point mutations have been found in cancer, only a small majority of these mutations have been shown to be causal. These rare driver mutations contribute to oncogenic signaling by altering pathways that are otherwise tightly regulated in normal tissues (*53*). It is known that cancer cells exhibit vast transcriptomic alterations and that cancer-specific isoforms are not merely by-products of abnormal physiology (*54*), yet most cancer-associated splicing choices, such as point mutations, are not oncogenic drivers.

Differential splicing choices allow for highly regulated expression of specific transcripts in normal development, yet expression of specific splice variants at developmentally inappropriate time points or in the wrong cell types may be detrimental. While it is known that aberrant splicing mechanisms exist in cancer (*55*–*57*), in this study, we show that a splice variant with a physiologic role in early organogenesis, but whose expression is not found in corresponding mature tissue, can be a driver of cancer. TrkB.T1 appears to be a candidate whose regulated splicing choice appears in normal embryonic development and whose misexpression at later postnatal time points is oncogenic.

While the embryogenic data offer correlative insight, the causal RCAS-TVA mouse studies show that aberrant expression of TrkB.T1 causes neoplasms at multiple primary sites, potentially by trapping cells in an undifferentiated state similar to their early embryogenic stage via interactions with known signaling pathways such as Wnt, SHH, TGF-β, or Ras. In the embryonic sci-RNA-seq3 data, TrkB.FL and TrkB.T1 are rarely, if ever, expressed in the same cell, and they also have a unique set of interactors as evidenced by HA AP-MS, suggesting that TrkB.T1 does not function through transactivation of TrkB.FL but potentially through other signaling pathways. In the context of tumors in vivo, however, there are many

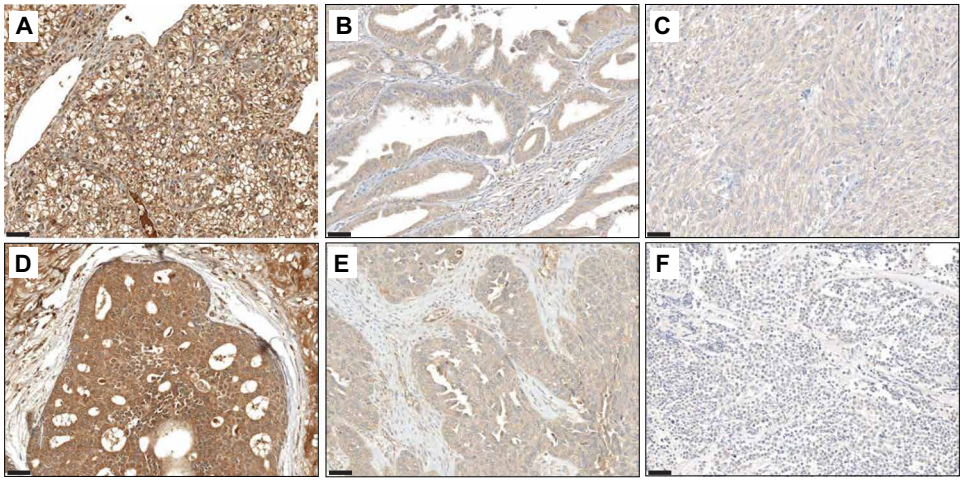

Fig. 6. TrkB.T1 has variable expression across multiple human tumor types. Representative micrographs of TrkB.T1 expression in (**A**) clear cell renal cell carcinoma, (**B**) colonic adenocarcinoma, (**C**) leiomyosarcoma, (**D**) mammary carcinoma (ductal carcinoma in situ is shown here), (**E**) pancreatic adenocarcinoma, and (**F**) seminoma. Scale bars, 100 μm.

endogenous receptor tyrosine kinases that could be influenced by the overexpression of TrkB.T1 during tumor initiation, maintenance, and metastasis. Future work should seek to address the precise interactors in vivo across a wide range of organ sites in a context- and cell-specific manner to expand upon initial experiments performed here in vitro with 3T3 cells and NSCs, to understand TrkB.T1's complex influences on endogenous tumor cell proliferation and growth.

These data highlight the TrkB.T1 splice variant as a promising candidate for future studies investigating the role of *NTRK2* in development and oncogenesis across a range of organ sites and tumor models beyond the known neurobiological roles of TrkB.T1 (*58*–*60*) and further strengthen the potential links between the tightly regulated splicing patterns of development with the aberrant splicing patterns observed in cancer. Approaches to studying splicing factors and alternatively spliced transcripts such as those delineated here should not be restricted to particular genes, stages of development, or organ sites and may uncover promising new avenues for diagnostics or therapeutics by revealing additional developmentally regulated, oncogenic splice variants.

METHODS

Bioinformatic analysis

Quantification of transcript data from sci-RNA-seq3

SAM (Sequence Alignment/Map) alignment files for the MOCA dataset were downloaded from https://shendure-web.gs.washington.edu/content/members/cao1025/public/nobackup/. The "cell_annotation.csv," which contained *t*-SNE coordinates, Uniform Manifold Approximation and Projection (UMAP) coordinates and information about clusters and trajectories, was downloaded from https://oncoscape.v3.sttrcancer.org/atlas.gs.washington.edu.mouse.rna/downloads. The "Comprehensive gene annotation" file was downloaded from www.gencodegenes.org/mouse/release_M12.html. For each of the 2,062,641 cells, we calculated the number of strand-specific unique molecular identifies (UMIs) for each cell mapping to transcripts of each gene with the Python v.2.7.13 HTSeq (*61*) package using GENCODE vM12 (*62*). Monocle3 (*63*) was used to construct a cell_data_set object with all the transcript expression data, and preprocess_cds() was used to normalize the transcript expression. The expression of TrkB.T1 and TrkB.FL was visualized over existing UMAPs and *t*-SNEs provided by Cao *et al.* (*40*) using ggplot2 (*64*). An interactive website (https://atlas.fredhutch.org/fredhutch/ntrk2/) has been put together to facilitate further exploration of the NTRK2 transcript data across various trajectories and cell types.

Obtaining and transforming transcript-level data from TCGA and TARGET

Transcript data (TCGA RNAseqV2 RSEM data) for TCGA and TARGET organ sites were downloaded from Broad's FireBrowse website (https://gdac.broadinstitute.org/). Transcript data (TPM data) were also downloaded for TARGET from UCSC Xena (https://xenabrowser.net/datapages/?dataset=target_RSEM_gene_tpm&host=https%3A%2F%2Ftoil.xenahubs.net&removeHub=https%3A%2F%2Fxena.treehouse.gi.ucsc.edu%3A443). The results published here are in whole or part based on data generated by TCGA (*43*) and the TARGET (https://ocg.cancer.gov/programs/target) initiative, phs000218. The data used for this analysis are available at https://portal.gdc.cancer.gov/projects.

To make the RSEM data from TCGA and TARGET and TPM data comparable, we converted RSEM counts from TCGA to TPM counts using the following formula (*65*): RSEM can be multiplied by 10^6. For transcript analyses, NTRK2 transcript IDs were manually aligned to confirm sequence homology and are as follows: TrkB.FL (UCSC, uc004aoa.1; Ensembl, ENST00000376213.1, NTRK2_201) and TrkB.T1 (UCSC, uc004aob.1; Ensembl, ENST00000395882.1, NTRK2_204). Transcript data were visualized using boxplots using R package ggplot2 (*64*). Gene fusions for all TCGA fusions were obtained from Genomic Data Commons portal (https://portal.gdc.cancer.gov/). The transcript levels for TrkB.T1 and N-terminal truncated TrkB.T1, both containing the 11–amino acid intracellular region, for TCGA samples IDs containing TRK gene fusions (including fusions in NTRK1, NTRK2, and NTRK3) were compared to the mean of all other NTRK transcripts.

AP-MS analysis

GO and Reactome pathway enrichment analysis for genes associated with enriched MS proteins (*66*, *67*) was done using R Bioconductor Packages clusterProfiler v 3.4.4 (*68*), and dot plots were made using R Bioconductor package DOSE.

Generation of murine tumors

The RCAS-TVA system used in this work has been described previously for murine tumor modeling in immunocompetent mice (*69*). DF-1 cells were transfected with the relevant RCAS viral plasmids using Extreme-Gene 9Transfection reagent (Roche) accordingly to the manufacturer's protocol. The cells were maintained for three passages, as described above to ensure viral propagation to all cells. After confirmation of RCAS-inserts by Western blot, DF-1 cells (passage 4 or later) were used for injection. Newborn *N/tv-a*;*Ink4a/Arf*$^{-/-}$ pups [postnatal day 0 (P0) to P1] were injected (Hamilton syringe #84877) with 1 μl of approximately 1×10^5 DF-1 cells infected with and producing relevant RCAS viruses suspended in serum-free Dulbecco's modified Eagle's medium (DMEM; TrkB.T1 and shPTEN) (*41*). Simultaneous delivery of two RCAS viruses was performed by the injection of 1 μl of approximately 2×10^5 DF-1 cells mixed with equal ratio. Mice were monitored for the duration of the study (250 days) to check for tumor-related symptoms such as palpable masses, lethargy, weight loss, seizure, hyperactivity, altered gait, poor grooming, macrocephaly, and paralysis. Mice with severe hydrocephalus presumably due to injection trauma or an inflammatory response against the DF-1 cells were excluded from survival analysis in this study. All animal experiments were approved by and conducted in accordance with the Institutional Animal Care and Use Committee of Fred Hutchinson Cancer Research Center (protocol #50842).

Mouse tissue processing

Mouse tissue (including normal tissue and solid tumors) was removed, fixed in 10% neutral-buffered formalin for a minimum of 72 hours, and embedded into paraffin blocks. Five-micrometer serial sections were cut from formalin-fixed paraffin-embedded specimens and mounted on slides.

Immunohistochemistry

Immunohistochemical staining was performed on 5-μm formalin-fixed/paraffin-embedded tissue sections using a Discovery XT Ventana Automated Stainer (Ventana Medical Systems Inc.), run using standard Ventana reagents and Vector secondaries for staining with the TrkB.T1 SPEH1_D12 scFv-Fc fusion (*44*) at 1:500 and PTEN

(Cell Signaling Technology, #9188, lot no. 4) at 1:100 or TrkB (kinase specific against amino acid 810; Abcam, #ab18987, lot no. GR3280550-2) at 1:250. All embryonic histology slides and human tissue microarray (BioMax, US, #BC001134b) slides were scanned using a Ventana DP200 slide scanning system (Roche Diagnostics) at ×20 magnification. Digital images of different organs during mouse development were analyzed using the Fiji image analysis software as described previously (*70*, *71*). Staining intensities in human tumor tissues were assessed using a semiquantitative *H* score system by multiplying the intensity of the stain (0, no staining; 1, weak staining; 2, moderate staining; 3, intense staining) by the percentage (0 to 100) of cells, showing staining intensity (*H* score range, 0 to 300) as described previously (*72*).

Flow cytometry

Rodent tumors were harvested and resuspended as single cells in phosphate-buffered saline (PBS)/0.3% bovine serum albumin. Cells were washed and incubated with the following antibodies: CD45-APC-Cy7 (BioLegend, clone 30-F11, catalog no. 103116, lot no. B242535), CD3e-PE (BD, clone 145-2C11, catalog no. 553061, lot no. 22126), GR1-PerCP (BD, clone Ly-6G/Ly-6C, catalog no. 552093, lot no. 73108), TER119-APC (BD, clone Ter-119, catalog no. 557909, lot no. 42622), B220–Alexa Fluor 647 (BD, clone RA3-6B2, catalog no. 557683, lot no. 22218), CD4-PerCP (BD, clone L3T3, catalog no. 553654, lot no. 60912), and CD8a-FITC (BD, clone Ly-2, catalog no. 553030, lot no. 46675), as indicated. Cells were analyzed on a custom-built LSR II flow cytometer (BD). Data compensation and analysis were performed using noncommercial software developed in our laboratory (*73*).

Soft agar colony formation assay

Lentiviral production

293T packaging cells were seeded in 100-mm plates at a density of 3.8×10^6 cells per plate. 293T cells were supplemented with complete DMEM (Thermo Fisher Scientific, catalog no. 11966025) containing 10% fetal bovine serum (Thermo Fisher Scientific, catalog no. 26140079) and 5% penicillin/streptomycin. 293T cells were split three times a week to maintain healthy density and incubated at 37°C. Once the optimal number of 293T 10-mm plates were produced, they were transfected with psPAX2 (Addgene, catalog no. 12260), pMD2.G (Addgene, catalog no. 12259), and the gene of interest containing pLJM1 lentiviral packaging plasmids (Addgene, catalog no. 91980) at concentrations of 1.3, 0.72, and 1.64 pmol. 293T cells were transfected using the Thermo Fisher Scientific Lipofectamine 3000 transfection protocol (Thermo Fisher Scientific, catalog no. L3000001). The medium was replaced after 18 hours to permit lentiviral production in transfection reagent–free medium.

Viral medium was harvested after 48, 72, and 96 hours and replaced with fresh medium after each harvest. The viral supernatant was filtered through 0.45-μm syringe filters Millex-HP Syringe Filter Unit 0.45 μm (MilliporeSigma, SLHP033RS) to remove cellular debris and other contaminants. NIH-3T3 cells were seeded in 100-mm plates at a density of 2.2×10^6 cells per plate and supplemented with complete DMEM containing 10% calf serum (Thermo Fisher Scientific, catalog no.16170086) and 5% penicillin/streptomycin. Once the NIH-3T3 plates reached optimal confluency, NIH-3T3 cells were supplemented with the viral harvest medium and left to incubate for 24 hours. The viral harvest was then removed and supplemented with fresh complete DMEM with puromycin (2 μg/ml). The NIH-3T3 cells were incubated for a week under these selection conditions until the population density rebounded to plate confluency.

Soft agar colony formation assay

Once the NIH-3T3 cells under each condition were confluent, we initiated the soft agar colony formation assay. A 3% agarose solution (Guidechem, catalog no. 9012-36-6) was microwaved for 1 min and stored in a 45°C water bath to maintain its liquid state. The 3% agarose solution was aliquoted and diluted with complete DMEM to yield a 0.6% agarose/medium solution. This new mixture was poured into six-well plates at 1 ml and allowed to solidify for 30 min. Aliquots of 0.6% solution were then diluted with the NIH-3T3 cell medium suspension so that the solution was composed of 0.3% agarose and contained a concentration of 2×10^3 cells/ml. This solution was stored at 37°C rather than 45°C to prevent cell death. The solution was plated atop the now solid 0.6% agarose layer and allowed to solidify at room temperature for 1 hour.

The agarose suspension of cells was incubated at 37°C for 30 days while supplemented with a 1-ml feeder layer of DMEM with puromycin (1 μg/ml) and 10% calf serum. After 30 days, the feeder layer was removed, and a solution of 0.005% crystal violet dye was plated onto the agarose to darken the formed colonies. Colonies were photographed at ×10 and ×20 magnifications and were counted at 4× magnification.

shTrkB.T1 and neurosphere formation

Real-time polymerase chain reaction

RNA from Nestin(N)/tv-a;Ink4a/Arf$^{-/-}$ neural progenitors was isolated using the RNeasy Kit (QIAGEN, catalog no. 74104), and 1 μg of total RNA was reverse transcribed using the high-capacity cDNA reverse transcription kit (Applied Biosystems, catalog no. 4368814). For quantitative analysis, we used the PowerUP SYBR Green Master Mix (Applied Biosystems, catalog no. A25742) following the manufacturer's instructions. Quantitative polymerase chain reaction (PCR) was performed using the QuantStudio 7 Real-Time PCR system. We have used previously published primers (*60*) for TrkB.T1 [AGCAATCGGGAGCATCTCT (forward) and TACCCATCCAGTGGGATCTT (reverse)] and TrkB.FL [AGCAATCGGGAGCATCTCT (forward) and CTGGCAGAGTCATCGTCGT (reverse)]. The threshold cycle number for the genes analyzed was normalized to actin [CGTGGGCCGCCCTAGGCACCA (forward) and CTTAGGGTTCAGGGGGGC (reverse)], and TrkB.FL and TrkB.T1 levels were normalized to uninfected (N)/tv-a;Ink4a/Arf$^{-/-}$ neural progenitors.

Neurosphere formation

Neural progenitors isolated from (N)/tv-a;Ink4a/Arf$^{-/-}$ pups at P0 as previously described (*33*) were infected with RCAS-PDGFB-shSCR (scrambled control) or RCAS-PDGFB-shRNA against TrkB.T1, using an RCAS-TVA system as has been described previously described (*41*, *69*). The specific hairpins against TrkB.T1 used in are as follows: shTrkB.T1#1 (GAAAAAGCTAACCACCTGCCCTTTAGATCTCTTGAATCTAAAGGGCAGGTGGTTAGCGGG), shTrkB.T1#2 (GAAAAAGCACTCTCCTCCGCTTTATCTTCTCTTGAAAGATAAAGCGGAGGAGAGTGCGGGGATC), and shTrkB.T1#3 (GAAAAAGTCATAAGATCCCCCTGGATTCTCTTGAAATCCAGGGGGATCTTATGACGGG), along with the scrambled control (GAAAAAGCTCTACAACCGCTCATCATATCTCTTGAATATGATGAGCGGTTGTAGAGCGGG).

Briefly, RCAS virus was produced in Chicken fibroblast (DF-1) cells maintained with 10% fetal bovine serum (Clonetech, catalog no. 631101) in DMEM (Thermo Fisher Scientific, catalog no.

11995-073) with 1% penicillin/streptomycin (Thermo Fisher Scientific, catalog no. 30-002-CI) at 39°C. DF-1 cells were transfected with the indicated RCAS plasmid using X-tremeGENE 9 DNA transfection reagent (Roche, catalog no. 06365809001) according to the manufacturer's protocol. RCAS transgene expression was confirmed via quantitative PCR analysis. DF-1 cells were then incubated with murine neurosphere medium for 24 hours to package the indicated RCAS plasmid into virus. Our murine neurosphere medium consisted of 45 ml of NeuroCult mouse basal medium (STEMCELL Technologies, catalog no. 05700), 5 ml of mouse NeuroCult proliferation supplement (STEMCELL Technologies, catalog no. 05701), 50 μl of epidermal growth factor (20 μg/ml; PeproTech Inc., catalog no. 100-47), 50 μl of basic fibroblast growth factor (10 μg/ml; PeproTech Inc., catalog no. 100-18B), 125 μl of heparin (STEMCELL Technologies, catalog no. 07980), and 500 μl of penicillin/streptomycin (Thermo Fisher Scientific, catalog no. 30-002-CI). This conditioned medium was then diluted 1:1 in fresh murine neurosphere medium and used to incubate (N)/tv-a;Ink4a/Arf$^{-/-}$ neural progenitor cells overnight. (N)/tv-a;Ink4a/Arf$^{-/-}$ neural progenitor cells were then washed with PBS and maintained in fresh neurosphere medium for 48 hours. They were then seeded at a concentration of 50,000 cells per well in ultralow attachment six-well plates (Corning, catalog no. 3471). Fresh neurosphere medium (0.5 ml per well) was added once a week. Neurospheres of >100 μm in diameter were manually counted using a Leica DMIL light-emitting diode (LED) microscope with an eyepiece graticule at 7, 14, and 21 days, and data were displayed for 21 days.

Representative bright-field (white-light LED) images of the sphere formation assay were obtained using the Dragonfly 200 High-speed Confocal Imaging Platform (Andor Technology Ltd.) on a Leica DMi8 microscope stand with Zyla 4.2 scientific complimentary metal-oxide semiconductor camera (Andor Technology Ltd.) and 10×/0.45–numerical aperture HC PL APO objective with the software Fusion version 2.3.0.36 (Oxford Instruments).

Affinity purification–mass spectrometry

Similar to methods for the colony formation assay, pLJM1 (Addgene) constructs containing the NTRK2 inserts of interest (TrkB.FL, TrkB.T1, or green fluorescent protein) were transfected into 293T cells, along with psPAX and pMD2.G packaging plasmids (Addgene), using polyethylenimine (Polysciences). Fresh medium was added 24 hours later, and viral supernatant was harvested 24 hours after that. For infection of 3T3 cells, 1×5^{10} cells per well were seeded into six-well plates. Lentivirus was used unconcentrated, and 24 hours after seeding, cells were infected at a multiplicity of infection of <1. Seventy-two hours after seeding, selection was begun for cells successfully expressing the constructs using puromycin (2 μg/ml; for 7 days).

3T3 cells were expanded after selection to create a stable line and collected for HA-tag coimmunoprecipitation (Co-IP) analysis (Pierce HA-Tag IP/Co-IP Kit, Thermo Fisher Scientific, catalog no. 26180) in M-Per buffer (M-PER Mammalian Protein Extraction Reagent, catalog no. 78501) 3 weeks after infection. This kit includes immobilized antibody resin and improved protocols over other methods with a GST-PI3K-SH2-HA fusion protein as positive control, is robust and specific, and has elution conditions compatible with subsequent downstream analysis. To remove detergents needed for Co-IP before downstream MS analysis, proteins were resolved by SDS–polyacrylamide gel electrophoresis (PAGE) (NuPAGE 10% bis/tris; LifeTech) according to XCell Sure Lock Mini-Cell's guidelines. Gels were stained with SimplyBlue SafeStain, and bands were excised and submitted to the Fred Hutch Proteomics Core for MS.

Gel slices were washed with water, 50% acetonitrile/50% water, acetonitrile, and ammonium bicarbonate (100 mM), followed by 50% acetonitrile/50% ammonium bicarbonate (100 mM). The solution was removed, and the gel slices were dried in a speed vac. The gel slices were reduced with dithiothreitol (10 mM in 100 mM ammonium bicarbonate) at 56°C for 45 min. The solution was removed and discarded. The gel slices were alkylated with 2-chloroacetamide (55 mM in 100 mM ammonium bicarbonate) and incubated in the dark at ambient temperature for 30 min. The solution was removed and discarded. The gel slices were washed with ammonium bicarbonate (100 mM) for 10 min on a shaker, and an equal amount of acetonitrile was added and continued to wash for 10 min on a shaker. The solution was removed and discarded, and the gel slices were dried in a speed vac for 45 min. The gel slices were cooled on ice, and a cold solution of trypsin (12.5 ng/μl; Promega, Madison, WI) in ammonium bicarbonate (100 mM) was added, enough to cover the gel slice. After 45 min, the trypsin solution was removed and discarded, and an equal amount of ammonium bicarbonate (50 mM) was added and incubated overnight at 37°C with mixing. Samples were spun down in a microfuge and the supernatants were collected. Peptides were extracted from the gel slices by adding 0.1% trifluoroacetic acid (TFA) enough to cover the slices and mixed at ambient temperature for 30 min. An equal amount of acetonitrile was added, and the samples were mixed for an additional 30 min. The samples were spun on a microfuge and the supernatants were pooled. The supernatants were concentrated in a speed vac. All samples were desalted using ZipTip C_{18} (Millipore, Billerica, MA) and eluted with 70% acetonitrile/0.1% TFA. The desalted material was concentrated in a speed vac.

The generated peptide samples were brought up in 2% acetonitrile in 0.1% formic acid (20 μl) and analyzed (18 μl) by liquid chromatography–electrospray ionization tandem MS (MS/MS) with a Thermo Fisher Scientific Easy-nLC 1000 (Thermo Fisher Scientific, Waltham, MA), coupled to a tribrid Orbitrap Fusion (Thermo Fisher Scientific, Waltham, MA) mass spectrometer. In-line desalting was accomplished using a reversed-phase trap column (100 μm by 20 mm) packed with Magic C_{18}AQ (5-μm 200-Å resin; Michrom Bioresources, Auburn, CA), followed by peptide separations on a reversed-phase column (75 μm by 250 mm) packed with ReproSil-Pur 120 C_{18}AQ (3-μm 120-Å resin; Dr. Maisch, Germany) directly mounted on the electrospray ion source. A 45-min gradient from 2 to 35% acetonitrile in 0.1% formic acid at a flow rate of 300 nl/min was used for chromatographic separations. A spray voltage of 2200 V was applied to the electrospray tip, and the Orbitrap Fusion instrument was operated in the data-dependent mode. MS survey scans were in the Orbitrap [ACG (automatic gain control) target value, 500,000; resolution, 120,000; injection time, 50 ms] with a 3-s cycle time, and MS/MS spectra acquisition were detected in the linear ion trap (AGC target value, 10,000; injection time, 35 ms) using higher-energy C-trap dissociation (HCD) activation with a normalized collision energy of 27%. Selected ions were dynamically excluded for 45 s after a repeat count of 1.

Data analysis was performed using Proteome Discoverer 2.5 (Thermo Fisher Scientific, San Jose, CA) using Sequest HT as the protein database search algorithm. The data were searched against a Uniprot Mouse (UP000000589 from 7 March 2021) database that included common contaminants (cRAPome 29 January 2015). Searches

were performed with settings for the proteolytic enzyme trypsin, and maximum missed cleavages were set to 2. The precursor ion tolerance was set to 10 parts per million, and the fragment ion tolerance was set to 0.5 Da. Variable modifications included oxidation on methionine (+15.995 Da) and carbamidomethyl on cysteine (+57.021 Da). All search results were run through Percolator for peptide validation, and peptide results were filtered to a 1% false discovery rate.

SUPPLEMENTARY MATERIALS

Supplementary material for this article is available at https://science.org/doi/10.1126/sciadv.abo6789

View/request a protocol for this paper from *Bio-protocol*.

REFERENCES AND NOTES

1. N. M. Aiello, B. Z. Stanger, Echoes of the embryo: Using the developmental biology toolkit to study cancer. *Dis. Model. Mech.* **9**, 105–114 (2016).
2. B. Yin, Z. Y. Ma, Z. W. Zhou, W. C. Gao, Z. G. du, Z. H. Zhao, Q. Q. Li, The TrkB+ cancer stem cells contribute to post-chemotherapy recurrence of triple-negative breast cancers in an orthotopic mouse model. *Oncogene* **34**, 761–770 (2015).
3. D. R. Gomez, L. A. Byers, M. Nilsson, L. Diao, J. Wang, L. Li, P. Tong, M. Hofstad, B. Saigal, I. Wistuba, N. Kalhor, S. Swisher, Y. Fan, W. K. Hong, M. Suraokar, C. Behrens, C. Moran, J. V. Heymach, Integrative proteomic and transcriptomic analysis provides evidence for TrkB (NTRK2) as a therapeutic target in combination with tyrosine kinase inhibitors for non-small cell lung cancer. *Oncotarget* **9**, 14268–14284 (2018).
4. C. B. de Farias, T. E. Heinen, R. P. dos Santos, A. L. Abujamra, G. Schwartsmann, R. Roesler, BDNF/TrkB signaling protects HT-29 human colon cancer cells from EGFR inhibition. *Biochem. Biophys. Res. Commun.* **425**, 328–332 (2012).
5. M. S. Kim, W. S. Lee, J. Jeong, S. J. Kim, W. Jin, Induction of metastatic potential by TrkB via activation of IL6/JAK2/STAT3 and PI3K/AKT signaling in breast cancer. *Oncotarget* **6**, 40158–40171 (2015).
6. G. M. Sclabas, S. Fujioka, C. Schmidt, Z. Li, W. A. I. Frederick, W. Yang, K. Yokoi, D. B. Evans, J. L. Abbruzzese, K. R. Hess, W. Zhang, I. J. Fidler, P. J. Chiao, Overexpression of tropomysin-related kinase B in metastatic human pancreatic cancer cells. *Clin. Cancer Res.* **11**, 440–449 (2005).
7. K. Makino, K. Kawamura, W. Sato, N. Kawamura, T. Fujimoto, Y. Terada, Inhibition of uterine sarcoma cell growth through suppression of endogenous tyrosine kinase B signaling. *PLOS ONE* **7**, e41049 (2012).
8. M. E. Kupferman, T. Jiffar, A. el-Naggar, T. Yilmaz, G. Zhou, T. Xie, L. Feng, J. Wang, F. C. Holsinger, D. Yu, J. N. Myers, TrkB induces EMT and has a key role in invasion of head and neck squamous cell carcinoma. *Oncogene* **29**, 2047–2059 (2010).
9. W. Bao, H. Qiu, T. Yang, X. Luo, H. Zhang, X. Wan, Upregulation of TrkB promotes epithelial-mesenchymal transition and anoikis resistance in endometrial carcinoma. *PLOS ONE* **8**, e70616 (2013).
10. R. N. Pearse, S. L. Swendeman, Y. Li, D. Rafii, B. L. Hempstead, A neurotrophin axis in myeloma: TrkB and BDNF promote tumor-cell survival. *Blood* **105**, 4429–4436 (2005).
11. X. Yu, L. Liu, B. Cai, Y. He, X. Wan, Suppression of anoikis by the neurotrophic receptor TrkB in human ovarian cancer. *Cancer Sci.* **99**, 543–552 (2008).
12. P. C. Lai, T. H. Chiu, Y. T. Huang, Overexpression of BDNF and TrkB in human bladder cancer specimens. *Oncol. Rep.* **24**, 1265–1270 (2010).
13. J. Lee, T. Jiffar, M. E. Kupferman, A novel role for BDNF-TrkB in the regulation of chemotherapy resistance in head and neck squamous cell carcinoma. *PLOS ONE* **7**, e30246 (2012).
14. K. W. Sinkevicius, C. Kriegel, K. J. Bellaria, J. Lee, A. N. Lau, K. T. Leeman, P. Zhou, A. M. Beede, C. M. Fillmore, D. Caswell, J. Barrios, K. K. Wong, L. M. Sholl, T. M. Schlaeger, R. T. Bronson, L. R. Chirieac, M. M. Winslow, M. C. Haigis, C. F. Kim, Neurotrophin receptor TrkB promotes lung adenocarcinoma metastasis. *Proc. Natl. Acad. Sci. U.S.A.* **111**, 10299–10304 (2014).
15. A. Eggert, M. A. Grotzer, N. Ikegaki, H. Zhao, A. Cnaan, G. M. Brodeur, A. E. Evans, Expression of the neurotrophin receptor TrkB is associated with unfavorable outcome in Wilms' tumor. *J. Clin. Oncol.* **19**, 689–696 (2001).
16. H. Yuzugullu, T. von, L. M. Thorpe, S. R. Walker, T. M. Roberts, D. A. Frank, J. J. Zhao, NTRK2 activation cooperates with PTEN deficiency in T-ALL through activation of both the PI3K-AKT and JAK-STAT3 pathways. *Cell Discov.* **2**, 16030 (2016).
17. Z. Li, Z. Chang, L. J. Chiao, Y. Kang, Q. Xia, C. Zhu, J. B. Fleming, D. B. Evans, P. J. Chiao, TrkBT1 induces liver metastasis of pancreatic cancer cells by sequestering Rho GDP dissociation inhibitor and promoting RhoA activation. *Cancer Res.* **69**, 7851–7859 (2009).
18. A. Vaishnavi, A. T. Le, R. C. Doebele, TRKing down an old oncogene in a new era of targeted therapy. *Cancer Discov.* **5**, 25–34 (2015).
19. A. Nakagawara, C. G. Azar, N. J. Scavarda, G. M. Brodeur, Expression and function of TRK-B and BDNF in human neuroblastomas. *Mol. Cell. Biol.* **14**, 759–767 (1994).
20. K. Moriwaki, Y. Ayani, H. Kuwabara, T. Terada, R. Kawata, M. Asahi, TRKB tyrosine kinase receptor is a potential therapeutic target for poorly differentiated oral squamous cell carcinoma. *Oncotarget* **9**, 25225–25243 (2018).
21. K. Okamura, T. Harada, S. Wang, K. Ijichi, K. Furuyama, T. Koga, T. Okamoto, K. Takayama, T. Yano, Y. Nakanishi, Expression of TrkB and BDNF is associated with poor prognosis in non-small cell lung cancer. *Lung Cancer* **78**, 100–106 (2012).
22. H. Akil, A. Perraud, M. O. Jauberteau, M. Mathonnet, Tropomyosin-related kinase B/brain derived-neurotrophic factor signaling pathway as a potential therapeutic target for colorectal cancer. *World J. Gastroenterol.* **22**, 490–500 (2016).
23. C. Zhang, X. Li, D. Gao, H. Ruan, Z. Lin, X. Li, G. Liu, Z. Ma, X. Li, The prognostic value of over-expressed TrkB in solid tumors: A systematic review and meta-analysis. *Oncotarget* **8**, 99394–99401 (2017).
24. J. P. Solomon, J. F. Hechtman, Detection of *NTRK* fusions: Merits and limitations of current diagnostic platforms. *Cancer Res.* **79**, 3163–3168 (2019).
25. Z. Gatalica, J. Xiu, J. Swensen, S. Vranic, Molecular characterization of cancers with NTRK gene fusions. *Mod. Pathol.* **32**, 147–153 (2019).
26. C. M. Albert, J. L. Davis, N. Federman, M. Casanova, T. W. Laetsch, TRK fusion cancers in children: A clinical review and recommendations for screening. *J. Clin. Oncol.* **37**, 513–524 (2019).
27. E. Cocco, M. Scaltriti, A. Drilon, NTRK fusion-positive cancers and TRK inhibitor therapy. *Nat. Rev. Clin. Oncol.* **15**, 731–747 (2018).
28. C. J. Desmet, D. S. Peeper, The neurotrophic receptor TrkB: A drug target in anti-cancer therapy? *Cell. Mol. Life Sci.* **63**, 755–759 (2006).
29. T. R. Geiger, D. S. Peeper, The neurotrophic receptor TrkB in anoikis resistance and metastasis: A perspective. *Cancer Res.* **65**, 7033–7036 (2005).
30. S. Douma, T. van Laar, J. Zevenhoven, R. Meuwissen, E. van Garderen, D. S. Peeper, Suppression of anoikis and induction of metastasis by the neurotrophic receptor TrkB. *Nature* **430**, 1034–1039 (2004).
31. M. A. Smit, D. S. Peeper, Zeb1 is required for TrkB-induced epithelial-mesenchymal transition, anoikis resistance and metastasis. *Oncogene* **30**, 3735–3744 (2011).
32. M. J. Contreras-Zárate, N. L. Day, D. R. Ormond, V. F. Borges, S. Tobet, B. Gril, P. S. Steeg, D. M. Cittelly, Estradiol induces BDNF/TrkB signaling in triple-negative breast cancer to promote brain metastases. *Oncogene* **38**, 4685–4699 (2019).
33. S. S. Pattwell, S. Arora, P. J. Cimino, T. Ozawa, F. Szulzewsky, P. Hoellerbauer, T. Bonifert, B. G. Hoffstrom, N. E. Boiani, H. Bolouri, C. E. Correnti, B. Oldrini, J. R. Silber, M. Squatrito, P. J. Paddison, E. C. Holland, A kinase-deficient *NTRK2* splice variant predominates in glioma and amplifies several oncogenic signaling pathways. *Nat. Commun.* **11**, 2977 (2020).
34. G. T. Baxter, M. J. Radeke, R. C. Kuo, V. Makrides, B. Hinkle, R. Hoang, A. Medina-Selby, D. Coit, P. Valenzuela, S. C. Feinstein, Signal transduction mediated by the truncated trkB receptor isoforms, trkB.T1 and trkB.T2. *J. Neurosci.* **17**, 2683–2690 (1997).
35. D. L. Shelton, J. Sutherland, J. Gripp, T. Camerato, M. P. Armanini, H. S. Phillips, K. Carroll, S. D. Spencer, A. D. Levinson, Human trks: Molecular cloning, tissue distribution, and expression of extracellular domain immunoadhesins. *J. Neurosci.* **15**, 477–491 (1995).
36. D. S. Middlemas, R. A. Lindberg, T. Hunter, trkB, a neural receptor protein-tyrosine kinase: Evidence for a full-length and two truncated receptors. *Mol. Cell Biol.* **11**, 143–153 (1991).
37. R. Klein, R. J. Smeyne, W. Wurst, L. K. Long, B. A. Auerbach, A. L. Joyner, M. Barbacid, Targeted disruption of the trkB neurotrophin receptor gene results in nervous system lesions and neonatal death. *Cell* **75**, 113–122 (1993).
38. K. Luberg, J. Wong, C. S. Weickert, T. Timmusk, Human TrkB gene: Novel alternative transcripts, protein isoforms and expression pattern in the prefrontal cerebral cortex during postnatal development. *J. Neurochem.* **113**, 952–964 (2010).
39. S. Biffo, N. Offenhauser, B. D. Carter, Y. A. Barde, Selective binding and internalisation by truncated receptors restrict the availability of BDNF during development. *Development* **121**, 2461–2470 (1995).
40. J. Cao, M. Spielmann, X. Qiu, X. Huang, D. M. Ibrahim, A. J. Hill, F. Zhang, S. Mundlos, L. Christiansen, F. J. Steemers, C. Trapnell, J. Shendure, The single-cell transcriptional landscape of mammalian organogenesis. *Nature* **566**, 496–502 (2019).
41. T. Ozawa, M. Riester, Y. K. Cheng, J. T. Huse, M. Squatrito, K. Helmy, N. Charles, F. Michor, E. C. Holland, Most human non-GCIMP glioblastoma subtypes evolve from a common proneural-like precursor glioma. *Cancer Cell* **26**, 288–300 (2014).
42. E. C. Holland, H. E. Varmus, Basic fibroblast growth factor induces cell migration and proliferation after glia-specific gene transfer in mice. *Proc. Natl. Acad. Sci. U.S.A.* **95**, 1218–1223 (1998).
43. The Cancer Genome Atlas Research Network, J. N. Weinstein, E. A. Collisson, G. B. Mills, K. R. M. Shaw, B. A. Ozenberger, K. Ellrott, I. Shmulevich, C. Sander, J. M. Stuart, The Cancer Genome Atlas Pan-Cancer analysis project. *Nat. Genet.* **45**, 1113–1120 (2013).
44. S. S. Pattwell, E. Q. Konnick, Y. J. Liu, R. A. Yoda, L. N. Sekhar, P. J. Cimino, *Neurotrophic Receptor Tyrosine Kinase 2 (NTRK2)* alterations in low-grade gliomas: Report of a novel

gene fusion partner in a pilocytic astrocytoma and review of the literature. *Case Rep. Pathol.* **2020**, 5903863 (2020).
45. T. Zhan, N. Rindtorff, M. Boutros, Wnt signaling in cancer. *Oncogene* **36**, 1461–1473 (2017).
46. Y. Sun, S. Pollard, L. Conti, M. Toselli, G. Biella, G. Parkin, L. Willatt, A. Falk, E. Cattaneo, A. Smith, Long-term tripotent differentiation capacity of human neural stem (NS) cells in adherent culture. *Mol. Cell. Neurosci.* **38**, 245–258 (2008).
47. S. M. Pollard, L. Conti, Y. Sun, D. Goffredo, A. Smith, Adherent neural stem (NS) cells from fetal and adult forebrain. *Cereb. Cortex* **16** (Suppl. 1), i112–i120 (2006).
48. J. H. Morris, G. M. Knudsen, E. Verschueren, J. R. Johnson, P. Cimermancic, A. L. Greninger, A. R. Pico, Affinity purification-mass spectrometry and network analysis to understand protein-protein interactions. *Nat. Protoc.* **9**, 2539–2554 (2014).
49. K. Ohira, K. J. Homma, H. Hirai, S. Nakamura, M. Hayashi, TrkB-T1 regulates the RhoA signaling and actin cytoskeleton in glioma cells. *Biochem. Biophys. Res. Commun.* **342**, 867–874 (2006).
50. K. Ohira, H. Kumanogoh, Y. Sahara, K. J. Homma, H. Hirai, S. Nakamura, M. Hayashi, A truncated tropomyosin-related kinase B receptor, T1, regulates glial cell morphology via Rho GDP dissociation inhibitor 1. *J. Neurosci.* **25**, 1343–1353 (2005).
51. C. R. Rose, R. Blum, B. Pichler, A. Lepier, K. W. Kafitz, A. Konnerth, Truncated TrkB-T1 mediates neurotrophin-evoked calcium signalling in glia cells. *Nature* **426**, 74–78 (2003).
52. Y. Nakamura, A. Suganami, M. Fukuda, M. K. Hasan, T. Yokochi, A. Takatori, S. Satoh, T. Hoshino, Y. Tamura, A. Nakagawara, Identification of novel candidate compounds targeting TrkB to induce apoptosis in neuroblastoma. *Cancer Med.* **3**, 25–35 (2014).
53. D. K. Simanshu, D. V. Nissley, F. McCormick, RAS proteins and their regulators in human disease. *Cell* **170**, 17–33 (2017).
54. E. El Marabti, I. Younis, The cancer spliceome: Reprograming of alternative splicing in cancer. *Front. Mol. Biosci.* **5**, 80 (2018).
55. A. Sveen, S. Kilpinen, A. Ruusulehto, R. A. Lothe, R. I. Skotheim, Aberrant RNA splicing in cancer; expression changes and driver mutations of splicing factor genes. *Oncogene* **35**, 2413–2427 (2016).
56. S. Oltean, D. O. Bates, Hallmarks of alternative splicing in cancer. *Oncogene* **33**, 5311–5318 (2014).
57. L. Escobar-Hoyos, K. Knorr, O. Abdel-Wahab, Aberrant RNA splicing in cancer. *Annu. Rev. Cancer Biol.* **3**, 167–185 (2019).
58. L. Carim-Todd, K. G. Bath, G. Fulgenzi, S. Yanpallewar, D. Jing, C. A. Barrick, J. Becker, H. Buckley, S. G. Dorsey, F. S. Lee, L. Tessarollo, Endogenous truncated TrkB.T1 receptor regulates neuronal complexity and TrkB kinase receptor function in vivo. *J. Neurosci.* **29**, 678–685 (2009).
59. S. G. Dorsey, C. L. Renn, L. Carim-Todd, C. A. Barrick, L. Bambrick, B. K. Krueger, C. W. Ward, L. Tessarollo, In vivo restoration of physiological levels of truncated TrkB.T1 receptor rescues neuronal cell death in a trisomic mouse model. *Neuron* **51**, 21–28 (2006).
60. G. Fulgenzi, F. Tomassoni-Ardori, L. Babini, J. Becker, C. Barrick, S. Puverel, L. Tessarollo, BDNF modulates heart contraction force and long-term homeostasis through truncated TrkB.T1 receptor activation. *J. Cell Biol.* **210**, 1003–1012 (2015).
61. S. Anders, P. T. Pyl, W. Huber, HTSeq—A Python framework to work with high-throughput sequencing data. *Bioinformatics* **31**, 166–169 (2015).
62. J. Harrow, A. Frankish, J. M. Gonzalez, E. Tapanari, M. Diekhans, F. Kokocinski, B. L. Aken, D. Barrell, A. Zadissa, S. Searle, I. Barnes, A. Bignell, V. Boychenko, T. Hunt, M. Kay, G. Mukherjee, J. Rajan, G. Despacio-Reyes, G. Saunders, C. Steward, R. Harte, M. Lin, C. Howald, A. Tanzer, T. Derrien, J. Chrast, N. Walters, S. Balasubramanian, B. Pei, M. Tress, J. M. Rodriguez, I. Ezkurdia, J. van Baren, M. Brent, D. Haussler, M. Kellis, A. Valencia, A. Reymond, M. Gerstein, R. Guigó, T. J. Hubbard, GENCODE: The reference human genome annotation for The ENCODE Project. *Genome Res.* **22**, 1760–1774 (2012).
63. C. Trapnell, D. Cacchiarelli, J. Grimsby, P. Pokharel, S. Li, M. Morse, N. J. Lennon, K. J. Livak, T. S. Mikkelsen, J. L. Rinn, The dynamics and regulators of cell fate decisions are revealed by pseudotemporal ordering of single cells. *Nat. Biotechnol.* **32**, 381–386 (2014).
64. H. Wickhaem, *Ggplot2: Elegant Graphics for Data Analysis*, Use R! (Springer, 2009), pp. viii, 212.
65. B. Li, C. N. Dewey, RSEM: Accurate transcript quantification from RNA-Seq data with or without a reference genome. *BMC Bioinformatics* **12**, 323 (2011).
66. B. Jassal, L. Matthews, G. Viteri, C. Gong, P. Lorente, A. Fabregat, K. Sidiropoulos, J. Cook, M. Gillespie, R. Haw, F. Loney, B. May, M. Milacic, K. Rothfels, C. Sevilla, V. Shamovsky, S. Shorser, T. Varusai, J. Weiser, G. Wu, L. Stein, H. Hermjakob, P. D'Eustachio, The Reactome pathway knowledgebase. *Nucleic Acids Res.* **48**, D498–D503 (2020).
67. A. Fabregat, S. Jupe, L. Matthews, K. Sidiropoulos, M. Gillespie, P. Garapati, R. Haw, B. Jassal, F. Korninger, B. May, M. Milacic, C. D. Roca, K. Rothfels, C. Sevilla, V. Shamovsky, S. Shorser, T. Varusai, G. Viteri, J. Weiser, G. Wu, L. Stein, H. Hermjakob, P. D'Eustachio, The Reactome Pathway Knowledgebase. *Nucleic Acids Res.* **46**, D649–D655 (2018).
68. G. Yu, L.-G. Wang, Y. Han, Q.-Y. He, clusterProfiler: An R package for comparing biological themes among gene clusters. *OMICS* **16**, 284–287 (2012).
69. E. C. Holland, J. Celestino, C. Dai, L. Schaefer, R. E. Sawaya, G. N. Fuller, Combined activation of Ras and Akt in neural progenitors induces glioblastoma formation in mice. *Nat. Genet.* **25**, 55–57 (2000).
70. J. Schindelin, I. Arganda-Carreras, E. Frise, V. Kaynig, M. Longair, T. Pietzsch, S. Preibisch, C. Rueden, S. Saalfeld, B. Schmid, J. Y. Tinevez, D. J. White, V. Hartenstein, K. Eliceiri, P. Tomancak, A. Cardona, Fiji: An open-source platform for biological-image analysis. *Nat. Methods* **9**, 676–682 (2012).
71. M. C. Haffner, D. M. Esopi, A. Chaux, M. Gürel, S. Ghosh, A. M. Vaghasia, H. Tsai, K. Kim, N. Castagna, H. Lam, J. Hicks, N. Wyhs, D. Biswal Shinohara, P. J. Hurley, B. W. Simons, E. M. Schaeffer, T. L. Lotan, W. B. Isaacs, G. J. Netto, A. M. de Marzo, W. G. Nelson, S. S. An, S. Yegnasubramanian, AIM1 is an actin-binding protein that suppresses cell migration and micrometastatic dissemination. *Nat. Commun.* **8**, 142 (2017).
72. M. C. Haffner, A. Chaux, A. K. Meeker, D. M. Esopi, J. Gerber, L. G. Pellakuru, A. Toubaji, P. Argani, C. Iacobuzio-Donahue, W. G. Nelson, G. J. Netto, A. M. de Marzo, S. Yegnasubramanian, Global 5-hydroxymethylcytosine content is significantly reduced in tissue stem/progenitor cell compartments and in human cancers. *Oncotarget* **2**, 627–637 (2011).
73. B. Wood, 9-color and 10-color flow cytometry in the clinical laboratory. *Arch. Pathol. Lab. Med.* **130**, 680–690 (2006).

Acknowledgments: We thank J. Yan, J. Zhang, D. Kumasaka, and D. Adair for continued technical and administrative assistance and support throughout these experiments. We thank F. S. Lee at Weill Cornell Medical College for advising on experiments and data. We thank P. Gafken and L. Jones of the Fred Hutchinson Proteomics Core for assistance in carrying out immunoprecipitation-MS experiments. We would also like to thank the Fred Hutchinson Cellular Imaging Shared Resource for assistance with microscopy and image analysis, especially L. Schroeder, CISR Acting Director. **Funding:** This research was supported by the Proteomics and Metabolomics Shared Resource of the Fred Hutch/University of Washington Cancer Consortium (P30 CA05704); the Cellular Imaging Shared Resource (CISR) of the Fred Hutch/University of Washington Cancer Consortium (P30 CA015704); NIH R01 CA195718 (to E.C.H.), U54 CA193461 (to E.C.H.), R01 CA100688 (to E.C.H.), T32 CA9657-25 (to S.S.P.), U54 DK106829 (to K.R.L. and S.S.P.), R21 CA223531 (to S.S.P.), and K08 CA245037 (to P.J.C.); Jacobs Foundation Research Fellowship (to S.S.P.); NSF Graduate Research Fellowship Program DGE-1762114 (to N.N.); Department of Defense W81XWH-20-1-0111 (to M.C.H); Safeway Foundation (to M.C.H.); The AACR-QuadW Foundation Fellowship for Clinical/Translational Sarcoma Research (to M.J.W.); the Kuni Foundation (to S.S.P. and M.J.W.); Paul G. Allen Frontiers Group Allen Discovery Center (to J.S.); and Howard Hughes Medical Institute (to J.S.). Autopsy materials used in this study were obtained from the University of Washington Neuropathology Core, which is supported by the Alzheimer's Disease Research Center (AG05136), the Adult Changes in Thought Study (AG006781), and Morris K Udall Center of Excellence for Parkinson's Disease Research (NS062684). **Author contributions:** S.S.P. proposed the scientific concepts, designed and performed experiments, generated data, assisted with bioinformatic analyses, and wrote the manuscript. S.A., H.B., and N.N. performed bioinformatic analyses, designed bioinformatic pipelines, and generated data. S.A., N.N., and M.Z. helped with data visualization. J.C. and J.S. contributed to the single-cell data and provided sci-RNA-seq3 expertise. P.J.C. and M.C.H. examined tissue slides for human and mouse, generated photomicrographs, offered neuropathology and general pathology expertise, and contributed to the manuscript. T.O. provided necessary reagents, supervised initial experimental design, and offered technical guidance throughout. K.R.L. performed experiments, generated data, and provided hematopoietic insight. N.C.H. and D.A.A.B. contributed to transformation experiments and collected data. M.J.W. helped with interpretation of sarcoma related data and manuscript preparation. F.S., V.V.P., and D.A.A.B. assisted with design, generation, and validation of RCAS vectors. N.R.-L. helped with MS experiments and subsequent data analysis. E.C.H. contributed to the overall experimental design, supervised the project, and offered critical feedback throughout the project and manuscript revisions. All authors discussed data and contributed to the final manuscript. **Competing interests:** The authors declare that they have no competing interests. **Data and materials availability:** The data and materials that support the findings of this study are included with the manuscript and supplemental data files. All R scripts used in this manuscript are freely available as an additional resource via https://zenodo.org/record/6629466 (DOI for upload: 10.5281/zenodo.6629465) and at https://github.com/sonali-bioc/Pattwell_transcript_sci-RNA-seq3.

Submitted 20 February 2022
Accepted 23 August 2022
Published 7 October 2022
10.1126/sciadv.abo6789